ANDERSON LOCALIZATION VS. MOTT–HUBBARD METAL–INSULATOR TRANSITION IN DISORDERED, INTERACTING LATTICE FERMION SYSTEMS

Krzysztof Byczuk,[*,†] Walter Hofstetter[‡] and Dieter Vollhardt[†]

[*] *Institute of Theoretical Physics,*
University of Warsaw, ul. Hoża 69,
PL-00-681 Warszawa, Poland

[†] *Theoretical Physics III,*
Center for Electronic Correlations and Magnetism,
Institute for Physics, University of Augsburg,
D-86135 Augsburg, Germany

[‡] *Institut für Theoretische Physik,*
Johann Wolfgang Goethe-Universität,
60438 Frankfurt/Main, Germany

We review recent progress in our theoretical understanding of strongly correlated fermion systems in the presence of disorder. Results were obtained by the application of a powerful nonperturbative approach, the dynamical mean-field theory (DMFT), to interacting disordered lattice fermions. In particular, we demonstrate that DMFT combined with geometric averaging over disorder can capture Anderson localization and Mott insulating phases on the level of one-particle correlation functions. Results are presented for the ground state phase diagram of the Anderson–Hubbard model at half-filling, both in the paramagnetic phase and in the presence of antiferromagnetic order. We find a new antiferromagnetic metal which is stabilized by disorder. Possible realizations of these quantum phases with ultracold fermions in optical lattices are discussed.

1. Introduction

In non-interacting quantum systems with disorder, e.g., in the presence of randomly distributed impurities, wavefunctions can either be spatially extended or localized. Until 1958 it was believed that a localized state corresponds to a bound state of an electron at the impurity. By contrast, in his landmark paper of 1958, Anderson[1] predicted that disorder can lead to quite a different type of localized state now referred to as "Anderson localized state". To understand its physical origin it should be noted that if a particle

is inserted into a disordered system it will start to spread. As a consequence the wave is backscattered by the impurities, leading to characteristic "weak localization" effects.[2–4] The multiple scattering of the electronic wave can enhance these perturbative effects to such a degree that the electrons become spatially localized; for reviews see Refs. 4–6. In this case there is a finite probability for an electron to return to the point where it was inserted. If states are extended, this probability is zero. So, in contrast to localized states bound at an impurity, Anderson localized states are confined to a region of space due to coherent backscattering from randomly distributed impurities.

In the thermodynamic limit the excitation spectrum determined from the resolvent of the one-particle system or the one-particle Green functions is very different for extended and localized states. The one-particle Green function describing an extended state has a branch cut on the real axis, and the spectrum of the Hamiltonian is continuous. By contrast, the Green function for a localized state has discrete poles located infinitely close to the real axis, which implies a discrete point spectrum of the Hamiltonian. In particular, the point-like spectrum of an Anderson localized state is dense.

In the presence of interactions between the electrons the same classification of (approximate) eigenstates may, in principle, be used. Namely, if the one-particle Green function of the interacting system has a branch cut at some energies, the states at those energies are extended. If the Green function has discrete, separate poles the corresponding states are bound states, and if the poles are discrete and lie dense the states are Anderson localized. Since one-particle wave functions are not defined in a many-body system, they cannot be employed to describe the localization properties of the system. Instead the reduced one-particle *density matrix*, or the one-particle Green function $G(\mathbf{r}-\mathbf{r}')$ in position representation, may be employed. For localized states these quantities approach zero for $|\mathbf{r}-\mathbf{r}'|\to\infty$. For extended states, their amplitude only fluctuates very weakly, i.e., of the order $1/V$, where V is the volume of the system.

In the following, we are interested in the question how states of many-body systems change when the interaction and/or the disorder are varied. In general, the very notion of a metal or an insulator is related to the properties of two-particle Green functions, e.g., the current- and density-correlation functions. There exist different approaches to study the disappearance of a diffusion pole at the metal–insulator transition, and correspondingly, the vanishing of the DC conductivity in the thermodynamic limit.[4,5,7,8] On physical grounds it is very plausible to expect that the presence of Anderson

localized states with dense, point-like spectrum at the Fermi level, discussed above in terms of one-particle Green function, implies zero conductivity. Mathematical proofs of this conjecture exist only for specific models and in limiting cases.[9] Indeed, it is usually assumed that the presence of Anderson localized states at the Fermi level implies the system to be an Anderson insulator, at least in the non-interacting case. This is also our line of approach which will be reviewed in this article.

The paper is structured as follows. In Sec. 2, we review general aspects of the interplay between interactions and disorder in lattice fermion systems. In particular, we discuss the important question concerning the appropriate average over the disorder, and describe the new developments in the field of cold atoms in optical lattices which will make it possible in the future to investigate disordered, interacting lattices fermions with unprecedented control over the parameters. The models of correlated fermions with disorder are introduced in Sec. 3, followed by an introduction into the dynamical mean-field theory (DMFT) (Sec. 4) and a more detailed discussion of arithmetic vs. geometric averaging over the disorder (Sec. 5). In Sec. 6, the DMFT self-consistency conditions for disordered systems are introduced. After having defined the characteristic quantities which help us to identify the different phases of the Anderson–Hubbard Hamiltonian (Sec. 7), the results for the ground state phase diagram at half-filling are reviewed (Sec. 8). In Sec. 9 the results are summarized.

2. Interplay between Interactions and Disorder in Lattice Fermion Systems

2.1. *Interactions vs. disorder*

The properties of solids are strongly influenced by the interaction between the electrons and the presence of disorder.[4,7,8] Namely, Coulomb correlations and randomness are both driving forces behind metal–insulator transitions (MITs) which involve the localization and delocalization of particles. While the electronic repulsion may lead to a Mott–Hubbard MIT,[7,10] the coherent backscattering of non-interacting particles from randomly distributed impurities can cause Anderson localization.[1,2]

Since electronic interactions and disorder can both (and separately) induce a MIT, one might expect their simultaneous presence to be even more effective in localizing electrons. However, this is not necessarily so. For example, weak disorder is able to weaken the effect of correlations since it redistributes states into the Mott gap and may thus turn an insulator into

a (bad) metal. Furthermore, short-range interactions lead to a transfer of spectral weight into the Hubbard subbands whereby the total band-width and thus the critical disorder strength for the Anderson MIT increases, implying a reduction of the effective disorder strength. Hence the interplay between disorder and interactions leads to subtle many-body effects,[4,8,11–17] which pose fundamental challenges for theory and experiment not only in condensed matter physics,[4,7,8,18,19] but most recently also in the field of cold atoms in optical lattices.[20–27] Indeed, ultracold gases have quickly developed into a fascinating new laboratory for quantum many-body physics.[20,21,28–33] A major advantage of cold atoms in optical lattices is the high degree of controllability of the interaction and the disorder strength, thereby allowing a detailed verification of theoretical predictions. The concepts, models, and techniques for their solution to be discussed in this paper equally apply to electronic systems and cold fermionic atoms in optical lattices. In the following we will therefore refer generally to the investigation of "correlated lattice fermion systems".

2.1.1. *Average over disorder*

In general, the theoretical investigation of disordered systems requires the use of probability distribution functions (PDFs) for the random quantities of interest. Indeed, in physical or statistical problems one is usually interested in "typical" values of random quantities which are mathematically given by the most probable value of the PDF.[34] However, in many cases the complete PDF is not known, i.e., only limited information about the system provided by certain averages (moments or cumulants) is available. In this situation it is very important to choose the most informative average of a random variable. For example, if the PDF of a random variable has a single peak and fast decaying tails the typical value of the random quantity is well estimated by its first moment, known as the *arithmetic* average (or arithmetic mean). But there are many examples, e.g., from astronomy, the physics of glasses or networks, economy, sociology, biology or geology, where the knowledge of the arithmetic average is insufficient since the PDF is so broad that its characterization requires infinitely many moments.[35,36] Such systems are called non-self-averaging. One example is Anderson localization: when a disordered system is close to the Anderson MIT,[1] most electronic quantities fluctuate strongly and the corresponding PDFs possess long tails which can be described by a log-normal distribution.[37–42] This is well illustrated by the local density of states (LDOS) of the disordered system. Most recently it was shown for various lattices in dimensions $d = 2$ and 3 that the system-size

dependence of the LDOS distribution is an unambigous sign of Anderson localization, and that the distribution of the LDOS of disordered electrons agrees with a log-normal distribution over up to ten orders of magnitude.[42] Therefore it is not surprising that the arithmetic mean of this random one-particle quantity does not resemble its typical value at all. In particular, it is non-critical at the Anderson transition[43–45] and hence cannot help to detect the localization transition. By contrast the *geometric* mean[35,36,46,47] of the LDOS, which represents the most probable ("typical") value of a log-normal distribution, is the appropriate average in this case. It vanishes at a critical strength of the disorder and hence provides an explicit criterion for Anderson localization in disordered systems,[1,39,42] even in the presence of interactions.[48,49]

2.1.2. *Dynamical mean-field approach to disordered systems*

In general, MITs occur at intermediate values of the interaction and/or disorder. Theories of MITs driven by interaction and disorder therefore need to be non-perturbative. Usually they cannot be solved analytically, and require numerical methods or self-consistent approximations. A reliable approximate method for the investigation of lattice fermions with a local interaction is provided by DMFT,[50–52] where the local single-particle Green function is determined self-consistently. If in this approach the effect of local disorder is taken into account through the arithmetic mean of the LDOS[53] one obtains, in the absence of interactions, the well-known coherent potential approximation (CPA).[54] However, the CPA does not describe the physics of Anderson localization since, as discussed above, the arithmetically averaged LDOS is non-critical at the Anderson transition.[45] To overcome this deficiency, Dobrosavljević and Kotliar[48] formulated a variant of the DMFT where the probability distributions (and not only the averages) of the local Green functions are determined self-consistently ("Statistical DMFT"). Employing a Slave–Boson mean-field theory as impurity solver, they investigated the disorder-driven MIT for infinitely strong repulsion off half-filling. This statistical approach was also employed in other studies of the Hubbard model[55] as well as in the case of electrons coupled to phonons[56] and the Falicov–Kimball model.[57] Subsequently, Dobrosavljević, Pastor and Nikolić[49] incorporated the geometrically averaged LDOS into the self–consistency cycle and thereby derived a mean-field theory of Anderson localization which reproduces many of the expected features of the disorder-driven MIT for non-interacting fermions. This scheme employs only one-particle quantities and is therefore easily incorporated into the DMFT

for disordered electrons in the presence of phonons,[56] or Coulomb correlations.[58–61]

2.2. *Cold atoms in optical lattices: a new realization of disordered, correlated lattice quantum gases*

During the last few years, cold atoms in optical lattices have emerged as a unique tool-box for highly controlled investigations of quantum many-body systems. In recent years, the level of control in applying disordered potentials to ultracold quantum gases has greatly improved.[23,24] Anderson localization in its pure form has been demonstrated by the expansion of weakly interacting Bose–Einstein condensates in a disordered speckle light field, giving rise to characteristic localized condensate wave functions with exponentially decaying tails.[25,26] The additional influence of strong repulsive interactions has been investigated recently in the first full experimental realization of the 3d disordered Bose–Hubbard model, by using a fine-grained optical speckle field superimposed by an optical lattice.[27] In this experiment a strong reversible suppression of the condensate fraction due to disorder was observed, indicating the formation of a disorder-induced insulating state. Independent experimental evidence was obtained from interacting ^{87}Rb bosons in a quasi-random (bichromatic) optical lattice, where a strong reduction of the Mott gap was found and interpreted as possible evidence for a compressible Bose glass phase.[22] On the theoretical side, low-dimensional quasi-disordered Bose systems have been successfully described by DMRG simulations,[62] which extended previous weak-coupling calculations and found a direct transition from superfluid to Mott insulator. Regarding disordered bosons in higher dimensions, the status of theory is still more controversial, although significant insight was gained by a new stochastic mean-field theory,[63] which allows for an efficient description of the Bose glass phase and has already provided phase diagrams for realistic speckle-type disorder[64] such as used experimentally.[27] Under debate remains the issue of a direct transition between Mott insulator and superfluid, which was claimed to be ruled out in recent QMC simulations in three spatial dimensions, supported by general heuristic arguments.[65] Regarding disordered fermions, while no experiments in cold gases have been performed yet, theory has significantly advanced in recent years, mostly due to progress in the application of DMFT to disordered and inhomogeneous systems.[48,49,58,60,66] The phase diagram of spin-1/2 lattice fermions in a random potential has now been determined theoretically, both in the

paramagnetic phase where Mott- and Anderson-insulator compete,[58] and in the low-temperature regime where antiferromagnetic ordering sets in and a new disorder-induced antiferromagnetic *metallic* phase was found.[60] In this way, predictions for single-particle spectral properties were also obtained, which are now becoming accessible experimentally via radio frequency spectroscopy measurements of strongly interacting fermionic quantum gases,[67] in analogy to photoemission spectroscopy of electronic solids. An alternative route towards single-particle spectroscopy based on stimulated Raman transitions has been discussed theoretically.[68] Very recently, also the dynamical structure factor of strongly interacting bosons in an optical lattice has been measured via two-photon Bragg scattering.[69,70] These new developments open the door towards controlled experimental realization and spectroscopy of strongly interacting and disordered fermions in optical lattices.

2.3. *Schematic phase diagram*

The Mott–Hubbard MIT is caused by short-range, repulsive interactions in the pure system and is characterized by the opening of a gap in the density of states at the Fermi level. By contrast, the Anderson MIT is due to the coherent backscattering of the quantum particles from randomly distributed impurities in a system without interactions; at the transition the character of the spectrum at the Fermi level changes from a continuous to a dense point spectrum. Already these two limits provide great challenges for theoretical investigations. It is an even greater challenge to explore the *simultaneous* presence of interactions and disorder in lattice fermions systems. In view of the construction of the dynamical mean-field approach employed here, the results which will be presented in the following are expected to provide a comprehensive description for systems in spatial dimensions $d = 3$ and larger, i.e., above the limiting dimension $d = 2$. Two particularly interesting questions are whether the metallic phase, which exists at weak enough disorder and/or interaction strength, will be reduced or enlarged, and whether the Mott and Anderson insulating phases are separated by a metallic phase. Corresponding schematic phase transition lines are shown in Fig. 1.1. It is plausible to assume that both MITs can be characterized by a single quantity, namely, the local density of states. Although the LDOS is not an order parameter associated with a symmetry breaking phase transition, it discriminates between a metal and an insulator which is driven by correlations and disorder.

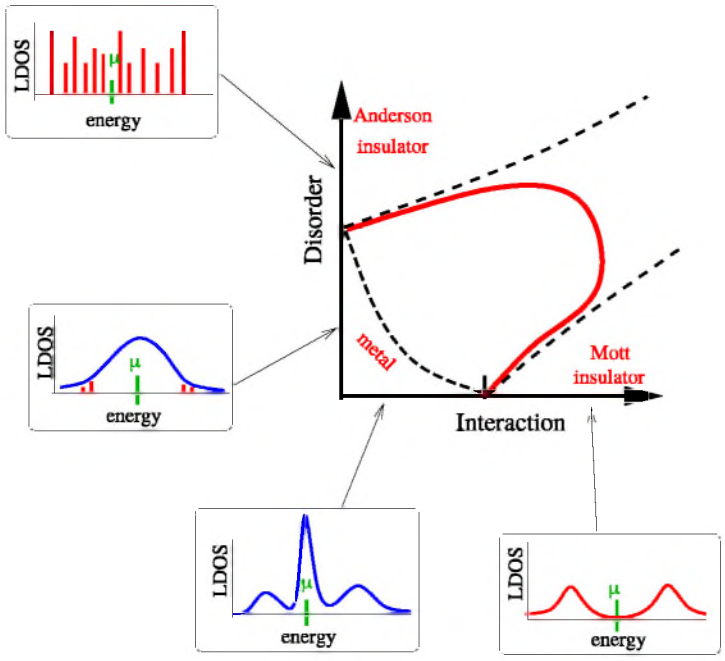

Fig. 1.1. Schematic diagram of the possible phases and shapes of phase transition lines in disordered, interacting lattice fermion systems. In principle, the interplay between interactions and disorder could reduce the metallic regime (dash-dotted line), or enlarge it (full and dashed lines). As will be discussed below, investigations within DMFT find that the metallic phase increases when interactions and disorder are simultaneously present (full line), and that the two insulating phases are connected continuously, i.e., without critical behavior. Insets show the local density of states in the absence of disorder or interaction, respectively.

3. Models of Correlated Fermions with Disorder

Here we study models of correlated fermions on ionic crystals or optical lattices in the presence of diagonal (i.e., local) disorder within a tight-binding description. In general, these models have the form

$$H = \sum_{ij\sigma} t_{ij\sigma} c^{\dagger}_{i\sigma} c_{j\sigma} + \sum_{i\sigma} \epsilon_i \, n_{i\sigma} + U \sum_{i} n_{i\uparrow} n_{i\downarrow} \tag{3.1}$$

where $c^{\dagger}_{i\sigma}$ and $c_{i\sigma}$ are the fermionic creation and annihilation operators of the particle with spin $\sigma = \pm 1/2$ at the lattice site i, $n_{i\sigma} = c^{\dagger}_{i\sigma} c_{i\sigma}$ is the particle number operator with eigenvalues 0 or 1, and $t_{ij\sigma}$ is the probability amplitude for hopping between lattice sites i and j. In the Hubbard model

$t_{ij\sigma} = t_{ij}$, i.e. the hopping amplitudes are the same for both spin projections. In the Falicov–Kimball model $t_{ij\sigma} = t_{ij}\delta_{\sigma\uparrow}$, i.e. only particles with one spin projection are mobile and the others are localized. The second term in (3.1) describes the additional external potential ϵ_i, which breaks the ideal lattice symmetry. For homogeneous systems we set $\epsilon_i = 0$, which defines the zero of the energy scale. The third term, a two-body term, describes the increase of the energy by $U > 0$ if two fermions with opposite spins occupy the same site. In Eq. (3.1) only a local part of the Coulomb interaction is included and other longer-range terms are neglected for simplicity. Note that this approximation is excellent in the case of cold gases in optical lattices, where the interaction between neutral atoms is essentially local.[28] The disorder affects the system through a local term $\sum_{i\sigma} \epsilon_i n_{i\sigma}$, where ϵ_i is a random variable drawn from a probability distribution function (PDF) $\mathcal{P}(\epsilon_1, \ldots, \epsilon_{N_L})$, where N_L is a number of lattice sites. Typically we consider uncorrelated, quenched disorder, where

$$\mathcal{P}(\epsilon_1, \ldots, \epsilon_{N_L}) = \prod_{i=1}^{N_L} P(\epsilon_i)\,. \tag{3.2}$$

Each of the $P(\epsilon_i)$ is the same, normalized PDF for the atomic energies ϵ_i. The quenched disorder means that $P(\epsilon_i)$ is time independent. In other words, the atomic energies ϵ_i are randomly distributed over the lattice and cannot fluctuate in time. This type of disorder is different from annealed disorder where the random atomic energies have thermal fluctuations.

In the following we use the continuous box-type PDF

$$P(\epsilon_i) = \frac{1}{\Delta}\Theta\left(\frac{\Delta}{2} - |\epsilon_i|\right)\,, \tag{3.3}$$

with $\Theta(x)$ as the Heaviside step function. The parameter Δ is therefore a measure of the disorder strength. The use of a different continuous, normalized function for the PDF would bring about only quantitative changes.

The Hubbard model and the Falicov–Kimball model defined by (3.1) are not only of interest for solid-state physics, but also in the case of ultracold atoms, where specific experimental realizations have been proposed.[20] By preparing a mixture of bosonic ^{87}Rb and fermionic ^{40}K in a 3d optical lattice, Ospelkaus *et al.* and Günter *et al.*[32] were able to create — to a first approximation — a version of the Falicov–Kimball model where the heavier bosonic species could be slowed down even further by using a species-dependent optical lattice and thus become "immobile" while the fermionic species remains mobile. Alternatively, if the heavy bosonic species could be frozen in a random configuration, this system would allow for a realization of the

Fermi–Hubbard model with quenched binary onsite disorder. A different approach towards quenched randomness in optical lattices was taken by White *et al.*[27] who implemented a fine-grained optical speckle potential superimposed onto a 3d optical lattice with interacting bosons and thus realized the bosonic version of the Anderson–Hubbard model (3.1) with continuous disorder. A third alternative approach to disordered cold gases is based on bichromatic optical lattices which are quasiperiodic, as implemented for the 3d Bose–Hubbard model by Fallani *et al.*[22] who observed a disorder-induced reduction of the Mott excitation gap, similar as discussed in the following for the fermionic case.

The Hamiltonian (3.1) is not solvable in general. Without disorder, i.e., for $\Delta = 0$, exact solutions on an arbitrary lattice and in arbitrary dimension exist only for $U = 0$ (non-interacting fermions), or $t_{ij\sigma} = 0$ (fermions in the atomic limit). In the $U = 0$ case the solution is obtained via discrete Fourier transform, i.e.,

$$H = \sum_{\mathbf{k}\sigma} \epsilon_{\mathbf{k}\sigma} c^\dagger_{\mathbf{k}\sigma} c_{\mathbf{k}\sigma}, \tag{3.4}$$

where $\epsilon_{\mathbf{k}\sigma} = \sum_{j(i)} t_{ij\sigma} e^{-i\mathbf{k}(\mathbf{R}_j - \mathbf{R}_i)}$ are free fermion dispersion relations. In the thermodynamic limit $N_L \to \infty$ the spectrum is continuous and eigenstates are extended. In the $t_{ij\sigma} = 0$ limit the lattice sites are uncorrelated and the exact partition function has the form $Z = \prod_i Z_i$, where

$$Z_i = 1 + 2e^{\beta\mu} + e^{-\beta U}, \tag{3.5}$$

where μ denotes the chemical potential within the grand canonical ensemble, and $\beta = 1/k_B T$ is the inverse temperature. In the thermodynamic limit the spectrum is point-like and the eigenstates are localized.

For finite disorder ($\Delta \neq 0$) an exact solution of the Hamiltonian (3.1) exists only for $t_{ij\sigma} = 0$. For a given realization of disorder, i.e., when all values of $\{\epsilon_1, \epsilon_2, \ldots, \epsilon_{N_L}\}$ are fixed, the partition function of the model (3.1) is given by

$$Z = \prod_i Z_i = \prod_i \left(1 + 2e^{-\beta(\epsilon_i - \mu)} + e^{-\beta U}\right). \tag{3.6}$$

As in the atomic limit discussed above ($t_{ij\sigma} = 0$) the spectrum is point-like in the thermodynamic limit and the eigenstates are localized.

The non-interacting limit ($U = 0$) of (3.1) with $t_{ij\sigma} \neq 0$ and disorder $\Delta \neq 0$ is not exactly solvable. In a seminal paper by Abou-Chacra, Thouless and Anderson[71] the model (3.1) with $U = 0$ and $t_{ij\sigma} = t$ between nearest neighbor sites was solved on the Bethe lattice, which is a tree-like

graph without loops.[40,72] The solution is expressed by the one-particle Green function

$$G_{ii}(\omega) = \langle i|\frac{1}{\omega - H}|i\rangle = \frac{1}{\omega - \epsilon_i - \eta_i(\omega)}, \tag{3.7}$$

where the hybridization function

$$\eta_i(\omega) = \sum_{j \neq i} \frac{t^2}{\omega - \epsilon_j - \eta_j(\omega)} \tag{3.8}$$

describes a resonant coupling of site i with its neighbors. If in the thermodynamic limit the imaginary part of $\eta_i(z)$ is finite in some band of energies z, then the states with energies z are extended. Otherwise, if the imaginary part of $\eta_i(z)$ is finite at discrete energies z such states are localized. For bound states these energies z form a point spectrum, and for Anderson localized states the energies z form a dense point-like spectrum in the thermodynamic limit. The analysis of the self-consistent equations derived for $\eta_i(z)$ by Abou-Chacra, Thouless, Anderson[71] showed that, indeed, continuous and dense point spectra are separated by a mobility edge which depends on the value of the disorder Δ.

In the following we solve the full Hamiltonian (3.1) by applying a dynamical mean-field approximation to deal with the interaction and then discuss how to cope with disorder.

4. Dynamical mean-field theory (DMFT)

The dynamical mean-field theory (DMFT) started from the following observation[50]: if the hopping amplitudes are scaled with fractional powers of the space dimension d (or the coordination number Z), i.e., $t = t^*/\sqrt{2d} = t^*/\sqrt{Z}$ for nearest neighbour hopping on a hypercubic lattice, then in the limit $d \to \infty$ ($Z \to \infty$) the self-energy $\Sigma_{ij}(\omega)$ in the Dyson equation

$$G_{ij\sigma}(i\omega_n)^{-1} = G^0_{ij\sigma}(i\omega_n)^{-1} - \Sigma_{ij\sigma}(i\omega_n), \tag{4.1}$$

(here in a real-space representation) becomes diagonal[73]

$$\Sigma_{ij\sigma}(i\omega_n) = \Sigma_{i\sigma}(i\omega_n)\, \delta_{ij}, \tag{4.2}$$

where $\omega_n = (2n+1)\pi/\beta$ are fermionic Matsubara frequencies. In a homogeneous system the self-energy is site independent, i.e., $\Sigma_{ij\sigma}(i\omega_n) = \Sigma_\sigma(i\omega_n)\, \delta_{ij}$, and is only a function of the energy. The DMFT approximation when applied to finite dimensional systems neglects off-diagonal parts

of the self-energy. In other words, the DMFT takes into account all temporal fluctuations but neglects spatial fluctuations between different lattice sites.[51,52]

Here we apply the DMFT to correlated fermion systems with disorder. Within DMFT we map a lattice site onto a single impurity, which is coupled to the dynamical mean-field bath. This coupling is represented by the hybridization function $\eta_{i\sigma}(\omega)$, which is determined self-consistently. The mapping is performed for all N_L lattice sites.

The partition function for a particular realization of disorder $\{\epsilon_1, \epsilon_2, \ldots, \epsilon_{N_L}\}$ is now expressed as a product of the partition functions which are determined for each impurity (representing lattice sites), i.e.,

$$Z = \prod_i Z_i = \prod_i \exp\left(\sum_{\sigma\omega_n} \ln[i\omega_n + \mu - \epsilon_i - \eta_{i\sigma}(\omega_n) - \Sigma_{i\sigma}(\omega_n)]\right) . \quad (4.3)$$

The mean-field hybridization function $\eta_{i\sigma}(\omega_n)$ is formally a site- and time-dependent one-particle potential. In the interaction representation, the unitary time evolution due to this potential is described by the local, time-dependent evolution operator[74,75]

$$U[\eta_{i\sigma}] = T_\tau e^{-\int_0^\beta d\tau \int_0^\beta d\tau' c^\dagger_{i\sigma}(\tau)\eta_{i\sigma}(\tau-\tau')c_{i\sigma}(\tau')} , \quad (4.4)$$

where $c_{i\sigma}(\tau)$ evolves according to the atomic part $H_i^{\rm loc}$ of the Hamiltonian (3.1) in imaginary Matsubara time $\tau \in (0, \beta)$, and T_τ is the time ordering operator. We write the partition function (4.3) as a trace over the operator

$$Z = Z[\eta_{i\sigma}] = \prod_{i=1}^{N_L} {\rm Tr}\left[e^{-\beta(H_i^{\rm loc} - \mu N_i^{\rm loc})} U[\eta_{i\sigma}]\right] , \quad (4.5)$$

where $N_i^{\rm loc}$ is the local particle number operator.

Equation (4.5) allows us to determine the local one-particle Green function $G_{ii\sigma}(\omega_n)$ for a given dynamical mean-field $\eta_{i\sigma}(\omega_n)$. Indeed, the local Green function is obtained by taking a functional logarithmic derivative of the partition function (4.5) with respect to $\eta_{i\sigma}(\omega_n)$, i.e.,

$$G_{ii\sigma}(\omega_n) = -\frac{\partial \ln Z[\eta_{i\sigma}]}{\partial \eta_{i\sigma}(\omega_n)} . \quad (4.6)$$

Then we find the local Dyson equations

$$\Sigma_{i\sigma}(\omega_n) = i\omega_n + \mu - \epsilon_i - \eta_{i\sigma}(\omega_n) - \frac{1}{G_{ii\sigma}(\omega_n)} , \quad (4.7)$$

for each N_L lattice sites. For a single realization of disorder $\{\epsilon_1, \epsilon_2, \ldots, \epsilon_{N_L}\}$, Eqs. (4.1), (4.2), (4.5)–(4.7) constitute a closed set of

equations. A solution of this set represents an approximate solution of the Hamiltonian (3.1).

5. Arithmetic vs. Geometric Averaging

A solution of Eqs. (4.1), (4.2), (4.5)–(4.7) is very difficult to obtain in practice. For each of the N_L impurities we need to determine the evolution operator (4.4) exactly. Using rigorous methods this can be done only for small N_L. However, Eqs. (4.1), (4.2), (4.5)–(4.7) should be solved in the thermodynamic limit, $N_L \to \infty$. This latter requirement might be overcome by performing a finite size scaling analysis. But such an analysis requires a large number of lattice sites N_L to reliably distinguish Anderson localized states from those belonging to the continuum. Here one faces a typical trade-off situation in computational physics. The computational problem is greatly reduced when the local interaction in (3.1) is factorized as in a Hartree–Fock approximation, whereby genuine correlations are eliminated.[15,76,77] Such approximate treatments can nevertheless provide valuable hints about the existence of particular phases. In our investigation[58–60] we employed the DMFT to include all local correlations as will be discussed in the next section.

If one could solve the DMFT equations exactly, one would obtain a set of local densities of states (LDOS)

$$A_{i\sigma}(\omega) = -\frac{1}{\pi}\mathrm{Im}G_{ii\sigma}(\omega_n \to \omega + i0^+)\,, \tag{5.1}$$

which are random quantities depending on the particular disorder realization $\{\epsilon_1,\ \epsilon_2,\ \ldots,\ \epsilon_{N_L}\}$. Usually one needs information about a system that does not depend on a particular disorder realization. Therefore one needs a statistical interpretation of the solutions of Eqs. (4.1), (4.2), (4.5)–(4.7).

When the system is large (cf., $N_L \to \infty$ in thermodynamic limit) one usually takes the arithmetic average of the LDOS $A_{i\sigma}(\omega)$ over many realizations of the disorder, i.e.,

$$\langle A_{i\sigma}(\omega)\rangle = \int \prod_{j=1}^{N_L} d\epsilon_j\ P(\epsilon_i)\ A_{i\sigma}(\omega; \{\epsilon_1, \ldots, \epsilon_{N_L}\})\,, \tag{5.2}$$

where the dependence on $\{\epsilon_1,\ \epsilon_2,\ \ldots,\ \epsilon_{N_L}\}$ is written explicitly. However, such a method holds only if the system is self-averaging. This means that sample-to-sample fluctuations

$$D_{N_L}(A_{i\sigma}(\omega)) = \frac{\langle A_{i\sigma}(\omega)^2\rangle - \langle A_{i\sigma}(\omega)\rangle^2}{\langle A_{i\sigma}(\omega)\rangle^2} \tag{5.3}$$

vanish for $N_L \to \infty$, which is equivalent to the central limit theorem for independent random variables $A_{i\sigma}(\omega)$. By performing the arithmetic average, one restores the translational invariance in the description of the disordered system, i.e., $A_\sigma(\omega)_{\rm arith} = \langle A_{i\sigma}(\omega)\rangle$ is the same for all lattice sites.

An example of a *non*-self-averaging system is a disordered system at the Anderson localization transition, or a system whose localization length is smaller than the diameter of the sample.[1] It implies that during the time evolution, a particle cannot explore the full phase space, i.e., cannot probe all possible random distributions. In such a case the arithmetic average (5.2) is inadequate. Here one is faced with the question concerning the proper statistical description of such a system.

The answer was given by Anderson[1]: one should investigate the full PDF for a given physical observable $P[A_{i\sigma}(\omega)]$ and find its most probable value, the "typical" value $A_\sigma(\omega)_{\rm typ}$, for which the PDF $P[A_{i\sigma}(\omega)]$ has a global maximum. The typical value of the LDOS, $A_\sigma(\omega)_{\rm typ}$, is the same for all lattice sites. By employing $A_\sigma(\omega)_{\rm typ}$ one restores translational invariance in the description of a disordered system. This value will represent typical properties of the system. Using photoemission spectroscopy one could, in principle, probe the LDOS at a particular lattice site and measure its most probable value. We note that if sample-to-sample fluctuations are small, the typical value $A_\sigma(\omega)_{\rm typ}$ would coincide with the arithmetic average $A_\sigma(\omega)_{\rm arith}$. On the other hand, in a non-self-averaging system the PDF can be strongly asymmetric, with a long tail, in which case the typical value $A_\sigma(\omega)_{\rm typ}$ would be very different from $A_\sigma(\omega)_{\rm arith}$. The arithmetic mean is strongly biased by rare fluctuations and hence does not represent the typical property of such a system.

Statistical approaches based on the computation of the probability distribution functions would require the inclusion of very many (perhaps infinitely many) impurity sites. This is very hard to achieve in practice, in particular, in correlated electron systems discussed here, although there have been recent successful attempts in this direction.[66] Therefore, one should look for a generalized average which yields the best approximation to the typical value. Among different means the *geometric* mean turns out to be very convenient to describe Anderson localization. The geometric mean is defined by

$$A_\sigma(\omega)_{\rm geom} = \exp\left[\langle \ln A_{i\sigma}(\omega)\rangle\right] , \tag{5.4}$$

where $\langle F(\epsilon_i)\rangle = \int \prod_i d\epsilon_i \mathcal{P}(\epsilon_i) F(\epsilon_i)$ is the arithmetic mean of the function $F(\epsilon_i)$. The geometric mean is an approximation to the most probable, typical

value of the LDOS

$$A_\sigma(\omega)_{\text{typ}} \approx A_\sigma(\omega)_{\text{geom}}. \tag{5.5}$$

It is easy to see that if $P[A_{i\sigma}(\omega)]$ is given by a log-normal PDF then $A_\sigma(\omega)_{\text{typ}} = A_\sigma(\omega)_{\text{geom}}$ holds exactly. It was shown that in the non-interacting case $A_\sigma(\omega)_{\text{geom}}$ vanishes at a critical strength of the disorder, hence providing an explicit criterion for Anderson localization.[1,39,48,49] We also note that by using the geometrically averaged LDOS we restore the translational invariance in our description of a disordered system. In addition, as we shall see in the next section, the restoration of translational invariance by averaging allows us to solve the DMFT equations in the thermodynamic limit. The problem of finite-size effects is then automatically absent.

6. DMFT Self-Consistency Conditions for Disordered Systems

According to the spectral theorem the geometrically averaged local Green function is given by

$$G_\sigma(\omega_n)_{\text{geom}} = \int d\omega \frac{A_\sigma(\omega)_{\text{geom}}}{i\omega_n - \omega}. \tag{6.1}$$

The DMFT self-consistency condition (4.6) is modified now to a translationally invariant form

$$\Sigma_\sigma(\omega_n) = i\omega_n + \mu - \eta_\sigma(\omega_n) - \frac{1}{G_\sigma(\omega_n)_{\text{geom}}}. \tag{6.2}$$

Here we assumed that $\langle \epsilon_i \rangle = 0$, which holds in particular for the box-shape PDF. We also used the translationally invariant hybridization function $\eta_\sigma(\omega_n)$. We can now perform a Fourier transform of the lattice Dyson equation (4.1) and obtain

$$G_\sigma(\omega_n)_{\text{geom}} = \int dz \frac{N_0(z)}{i\omega_n - z + \mu - \Sigma_\sigma(\omega_n)}, \tag{6.3}$$

where $N_0(z)$ is the density of states for a non-interacting and non-disordered lattice system.

Altogether the solution of the DMFT equations for interacting fermions with disorder requires the following steps:

(1) Select (i) N_L values of ϵ_i from a given PDF $P(\epsilon_i)$, (ii) an initial hybridization function $\eta_\sigma(\omega_n)$, and (iii) an initial self-energy $\Sigma_\sigma(\omega_n)$;

(2) for each ϵ_i solve the impurity problem defined by Eqs. (4.4)–(4.6);
(3) determine the LDOS $A_{i\sigma}(\omega)$ from the imaginary part of $G_{ii\sigma}(\omega)$, and $A_\sigma(\omega)_{\text{geom}}$ from Eq. (5.4);
(4) employ (6.1) to find $G_\sigma(\omega_n)_{\text{geom}}$;
(5) from Eqs. (6.2) and (6.3) find a new $\eta_\sigma(\omega_n)$ and $\Sigma_\sigma(\omega_n)$, then go to step (2) until convergence is reached.

It is clear that due to the averaging procedure we restore both translational invariance and the thermodynamic limit although N_L is finite. Therefore the method is superior to other stochastic methods which are affected by finite size effects.

In the presence of antiferromagnetic long-range order the self-consistency conditions are modified. In this case we introduce two sublattices s =A or B, and calculate two local Green functions $G_{ii\sigma s}(\omega_n)$. From this quantity we obtain the geometrically averaged LDOS $A_{\sigma s}(\omega)_{\text{geom}} = \exp\left[\langle \ln A_{i\sigma s}(\omega)\rangle\right]$, where $A_{i\sigma s}(\omega)$ is given as shown in Eq. (5.1). The local Green function is then obtained from the Hilbert transform (6.1). The local self-energy $\Sigma_{\sigma s}(\omega)$ is determined from Eq. (6.2). The self-consistent DMFT equations are closed by the Hilbert transform of the Green function on a bipartite lattice:

$$G_{\sigma s}(\omega_n)_{\text{geom}} = \int dz \, \frac{N_0(z)}{\left[i\omega_n - \Sigma_{\sigma s}(\omega_n) - \frac{z^2}{i\omega_n - \Sigma_{\sigma \bar{s}}(\omega_n)}\right]}. \tag{6.4}$$

Here $\bar{s}$ denotes the sublattice opposite to s.[51,53]

We note that if the geometric mean were replaced by the arithmetic mean one would obtain a theory where disorder effects are described only on the level of the CPA, which cannot detect Anderson localization. It should also be pointed out that in the presence of disorder the LDOS represented by $A_\sigma(\omega)_{\text{geom}}$ is not normalized to unity. This means that $A_\sigma(\omega)_{\text{geom}}$ only describes the extended states of the continuum part of the spectrum. Localized states, which have a dense point spectrum, are not included in the DMFT with geometric average. Therefore, this approach cannot describe the properties of the Anderson-insulator phase.

The accuracy of the DMFT approach with geometric average over disorder was checked against numerically exact results obtained for non-interacting fermions on a cubic lattice.[49,78] The critical disorder strengths at which Anderson localization occurs were found to agree within a factor of two[78] or better.[49] However, there exists a discrepancy regarding the shape of the mobility edge, which shows a pronounced reentrant behavior for non-interacting particles with box-type PDF of the disorder. This feature is not reproduced by our approach.[78] On the other hand, the re-entrant behavior

is a non-universal feature. Namely, it is much less pronounced in the case of a Gaussian PDF for disorder, and does not occur at all for a Lorentzian PDF.[79]

It should be pointed out that the DMFT-based self-consistent approach to interacting lattice fermions with disorder discussed here, is not related to the self-consistent theory of Anderson localization by Vollhardt and Wölfle[5] and its generalizations.[80,81] Namely, the latter theory determines the frequency dependent diffusion coefficient $D(\omega)$ from arithmetically averaged two-particle correlation functions by considering diffuson and cooperon diagrams. The approach reviewed here does not make use of these coherent back-scattering contributions, but computes a one-particle correlation function, the LDOS, and thereby extracts information on Anderson localization. The fact that the DMFT is based on a local approximation through the limit of large spatial dimensions does not necessarily imply that back-scattering contributions are entirely absent in this approach. Indeed, contributions due to back-scattering are implicitly contained in the hybridization function, which describes the diffusion of one-particle excitations away from and back to a given lattice site.[1,71] Quite generally the relation between theoretical approaches based on one-particle and two-particle correlation functions, respectively, and their results for the critical disorder strength for Anderson localization, is still not sufficiently understood and will continue to be an important topic for future research. Perhaps the limit of high lattice dimensions will serve as a useful starting point.[54,82,83]

7. Identification of Different Phases

To characterize the ground state of the Hamiltonian (3.1) the following quantities are computed:

(1) the LDOS $A_{\sigma s}(\omega)_{\text{geom}}$ for a given sublattice s and spin direction σ;
(2) the total DOS for a given sublattice s at the Fermi level ($\omega = 0$) with $N_s(0)_{\text{geom}} \equiv \sum_\sigma A_{\sigma s}(\omega = 0)_{\text{geom}}$;
(3) the staggered magnetization $m_{\text{AF}}^{\text{geom}} = |n_{\uparrow A}^{\text{geom}} - n_{\uparrow B}^{\text{geom}}|$, where $n_{\sigma s}^{\text{geom}} = \int_{-\infty}^{0} d\omega A_{\sigma s}(\omega)_{\text{geom}}$ is the local particle density on sublattice s.[84]

For comparison we determine these quantities also with the arithmetic average.

The possible phases of the Anderson–Hubbard model can then be classified as follows: The systems is a

- paramagnetic metal if $N_s^{\text{geom}}(0) \neq 0$ and $m_{\text{AF}}^{\text{geom}} = 0$;

- AF metal if $N_s^{\mathrm{geom}}(0) \neq 0$ and $m_{\mathrm{AF}}^{\mathrm{geom}} \neq 0$;
- AF insulator if $N_s^{\mathrm{geom}}(0) = 0$ and $m_{\mathrm{AF}}^{\mathrm{geom}} \neq 0$ but $N_s^{\mathrm{geom}}(\omega) \neq 0$ for some $\omega \neq 0$ (in fact, the last condition is already implied by $m_{\mathrm{AF}}^{\mathrm{geom}} \neq 0$);
- paramagnetic Anderson–Mott insulator if $N_s^{\mathrm{geom}}(\omega) = 0$ for all ω.

Note, that we use the term "metal" also for neutral fermionic atoms if they fulfil the above conditions.

8. Ground State Phase Diagram of Interacting, Disordered Lattice Fermion Systems at Half-Filling

We now apply the formalism discussed above to the Anderson–Hubbard model at half-filling and compare the ground state properties in the paramagnetic and magnetic cases.[58,60]

In the following we choose a model DOS, $N_0(\epsilon) = 2\sqrt{D^2 - \epsilon^2}/\pi D^2$, with bandwidth $W = 2D$, and set $W = 1$. For this DOS and for a bipartite lattice, the local Green function and the hybridization function are connected by the simple algebraic relation $\eta_{\sigma s}(\omega)_{\mathrm{geom}} = D^2 G_{\sigma\bar{s}}(\omega)_{\mathrm{geom}}/4$.[51]

The DMFT equations are solved at zero temperature by the numerical renormalization group technique,[85] which allows us to calculate the geometric or arithmetic average of the local DOS in each iteration loop.

8.1. *Paramagnetic phase diagram*

The ground state phase diagram of the Anderson–Hubbard model at half-filling obtained within the DMFT approach discussed above is shown in Fig. 1.2.[58] Two different phase transitions are found to take place: a Mott–Hubbard MIT for weak disorder Δ, and an Anderson MIT for weak interaction U. The correlated, disordered metal is surrounded by two different insulating phases whose properties, as well as the transitions between them, will now be discussed. In this section, the spin index σ is omitted since all quantities are spin independent.

(*i*) *Disordered, metallic phase* — The correlated, disordered metal is characterized by a non-zero value of the spectral density at the Fermi level, $A(\omega = 0)_{\mathrm{geom}} \neq 0$. In the absence of disorder, DMFT predicts this quantity to be given by the bare DOS $N_0(0)$, which is a consequence of the Luttinger theorem. This means that Landau quasiparticles are well-defined at the Fermi level. The situation changes completely when disorder is introduced since a subtle competition between disorder and electron interaction arises.

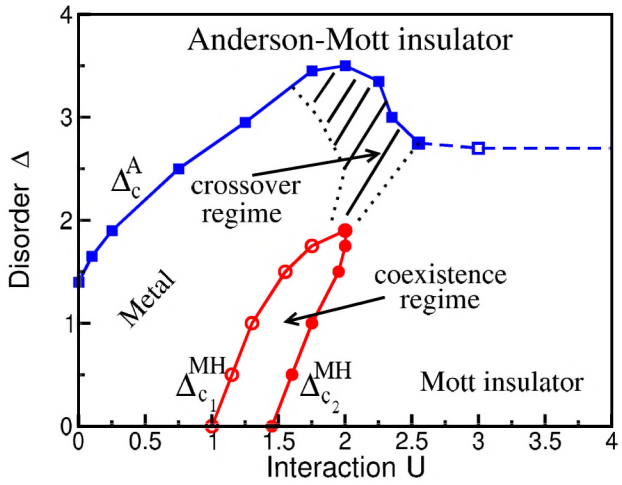

Fig. 1.2. Non-magnetic ground state phase diagram of the Anderson–Hubbard model at half-filling as calculated by DMFT with the typical local density of states; after Ref. 58.

Increasing the disorder strength at fixed U reduces $A(0)_{\rm geom}$ and thereby decreases the metallicity as shown in the upper panel left of Fig. 1.3. The opposite behavior is found when the interaction is increased at fixed Δ (see right panel of Fig. 1.3 for $\Delta = 1$), i.e., in this case the metallicity improves. In the strongly interacting metallic regime the value of $A(0)_{\rm geom}$ is restored, reaching again its maximal value $N_0(0)$. This implies that in the metallic phase sufficiently strong interactions protect the quasiparticles from decaying by impurity scattering. For weak disorder this interaction effect is almost independent of how the LDOS is averaged.

(*ii*) *Mott–Hubbard MIT* — For weak to intermediate disorder strength there is a sharp transition at a critical value of U between a correlated metal and a gapped Mott insulator. Two transition lines are found depending on whether the MIT is approached from the metallic side [$\Delta_{c2}^{MH}(U)$, full dots in Fig. 1.2] or from the insulating side [$\Delta_{c1}^{MH}(U)$, open dots in Fig. 1.2]. The hysteresis is clearly seen in right panel of Fig. 1.3 for $\Delta = 1$. The curves $\Delta_{c1}^{MH}(U)$ and $\Delta_{c2}^{MH}(U)$ in Fig. 1.2 are seen to have positive slope. This is a consequence of the disorder-induced increase of spectral weight at the Fermi level which in turn requires a stronger interaction to open the correlation gap. In the Mott insulating phase close to the hysteretic region an increase of disorder will therefore drive the system *back* into the metallic phase. The corresponding abrupt rise of $A(0)_{\rm geom}$ is clearly seen in the left lower panel

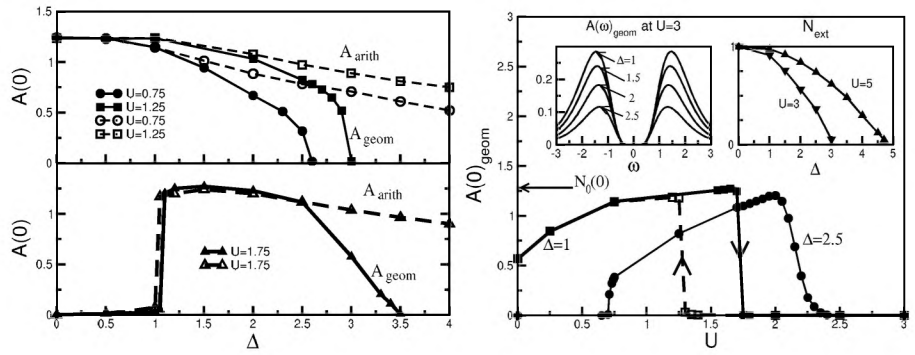

Fig. 1.3. Left panel: local density of states (LDOS) as a function of disorder Δ for various values of the interaction U. Solid (dashed) curves correspond to the geometrically (arithmetically) averaged LDOS. Right panel: geometrically averaged LDOS as a function of interaction U for different disorder strengths Δ. Solid (dashed) curves with closed (open) symbols are obtained with an initial metallic (insulating) hybridization function. Triangles: $\Delta = 1$; dots: $\Delta = 2.5$. Left inset: LDOS with Mott gap at $U = 3$ for different disorder strengths Δ. Right inset: integrated LDOS N_{geom} as a function of Δ at $U = 3$; after Ref. 58.

of Fig. 1.3. In this case the disorder protects the metal from becoming a Mott insulator.

Around $\Delta \approx 1.8$ the curves $\Delta_{c1}^{MH}(U)$ and $\Delta_{c2}^{MH}(U)$ terminate at a single critical point, cf. Fig. 1.2. For stronger disorder ($\Delta \gtrsim 1.8$) there appears to be a smooth crossover rather than a sharp transition from the metal to the insulator. This is illustrated by the U dependence of $A(0)_{\mathrm{geom}}$ shown in right panel of Fig. 1.3 for $\Delta = 2.5$. In this parameter regime the Luttinger theorem is not obeyed for any U. In the crossover regime, marked by the hatched area in Fig. 1.2, $A(0)_{\mathrm{geom}}$ vanishes gradually, so that the metallic and insulating phases can no longer be distinguished rigorously.[86]

Qualitatively, we find that the Mott–Hubbard MIT and the crossover region do not depend much on the choice of the average of the LDOS.[87] We also note the similarity between the Mott–Hubbard MIT scenario discussed here for disordered systems and that for a system without disorder at *finite* temperatures,[51,86] especially the presence of a coexistence region with hysteresis. However, while in the non-disordered case the interaction needed to trigger the Mott–Hubbard MIT decreases with increasing temperature, the opposite holds in the disordered case.

(*iii*) *Anderson MIT* — The metallic phase and the crossover regime are found to lie next to an Anderson insulator phase where the LDOS of the

extended states vanishes completely (see Fig. 1.2). The critical disorder strength $\Delta_c^A(U)$ corresponding to the Anderson MIT is a non-monotonous function of the interaction: it increases in the metallic regime and decreases in the crossover regime. Where $\Delta_c^A(U)$ has a positive slope an increase of the interaction turns the Anderson insulator into a correlated metal. This is illustrated in Fig. 1.3 for $\Delta = 2.5$; at $U/W \approx 0.7$ a transition from a localized to a metallic phase occurs, i.e., the spectral weight at the Fermi level becomes finite. In this case the electronic correlations inhibit the localization of quasiparticles by scattering at the impurities.

Figure 1.3 shows that the Anderson MIT is a continuous transition. In the critical regime $A(0)_{\text{geom}} \sim [\Delta_c^A(U) - \Delta]^\beta$ for $U = \text{const}$. In the crossover regime a critical exponent $\beta = 1$ is found (see the case $U = 1.75$ in lower panel of Fig. 1.3); elsewhere $\beta \neq 1$. However, we cannot rule out a very narrow critical regime with $\beta = 1$ since it is difficult to determine β with high accuracy. It should be stressed that an Anderson transition with vanishing $A(0)_{\text{geom}}$ at finite $\Delta = \Delta_c^A(U)$ can only be detected within DMFT when the geometrically averaged LDOS is used (solid lines in Fig. 1.3). Indeed, using arithmetic averaging one finds a nonvanishing LDOS at any finite Δ (dashed lines in Fig. 1.3).

(*iv*) *Mott and Anderson insulators* — The Mott insulator (with a correlation gap) is rigorously defined only in the absence of disorder ($\Delta = 0$), and the gapless Anderson insulator only for non-interacting systems ($U = 0$) and $\Delta > \Delta_c^A(0)$. For finite interactions and disorder this distinction can no longer be made. On the other hand, as long as the LDOS shows the characteristic Hubbard subbands (left inset in Fig. 1.3) one may refer to a *disordered Mott insulator*. With increasing disorder Δ, the spectral weight of the Hubbard subbands vanishes (right inset in Fig. 1.3) and the system becomes a *correlated Anderson insulator*. The boundary between these two types of insulators is marked by a dashed line in Fig. 1.2. The results obtained here within DMFT show that the paramagnetic Mott and Anderson insulators are continuously connected. Hence, by changing U and Δ it is possible to move from one insulating state to another one without crossing a metallic phase.

8.2. *Magnetic phase diagram*

At half-filling and in the absence of frustration effects interacting fermions order antiferromagnetically. This raises several basic questions: (i) how is a non-interacting, Anderson localized system at half filling influenced by a local interaction between the particles? (ii) how does an antiferromagnetic

(AF) insulator at half filling respond to disorder which in the absence of interactions would lead to an Anderson localized state? (iii) do Slater and Heisenberg antiferromagnets behave differently in the presence of disorder? Here we provide answers to these questions by calculating the zero temperature, magnetic phase diagram of the disordered Hubbard model at half filling using DMFT together with a geometric average over the disorder and allowing for a spin-dependence of the DOS.[60]

The ground state phase diagram of the Anderson–Hubbard model (3.1) obtained by the above classification is shown in Fig. 1.4. Depending on whether the interaction U is weak or strong the response of the system to disorder is found to be very different. In particular, at strong interactions, $U/W \gtrsim 1$, there exist only two phases, an AF insulating phase at weak disorder, $\Delta/W \lesssim 2.5$, and a paramagnetic Anderson–Mott insulator at strong disorder, $\Delta/W \gtrsim 2.5$. The transition between these two phases is continuous. Namely, the local DOS and the staggered magnetization both decrease gradually as the disorder Δ increases and vanish at their mutual boundary (lower panel of Fig. 1.5). By contrast, the phase diagram for weak interactions, $U/W \lesssim 1$, has a much richer structure (Fig. 1.4). In particular, for weak disorder a *paramagnetic* metallic phase is stable. It is separated from the AF insulating phase at large U by a narrow region of *AF metallic* phase. The AF metallic phase is long-range ordered, but there is no gap since the disorder leads to a redistribution of spectral weight.[60]

To better understand the nature of the AF phases in the phase diagram we take a look at the staggered magnetization m^{α}_{AF}. The dependence of $m^{\mathrm{geom}}_{\mathrm{AF}}$ on U is shown in the upper panel of Fig. 1.5 for several values of the disorder Δ. In contrast to the non-disordered case a finite interaction strength $U > U_c(\Delta)$ is needed to stabilize the AF long-range order when disorder is present. The staggered magnetization saturates at large U for both averages; the maximal values depend on the disorder strength. In the lower panel of Fig. 1.5, the dependence of m^{α}_{AF} on the disorder Δ is shown for different interactions U. Only for small U do the two averages yield approximately the same results.

Another useful quantity is the polarization $P^{\alpha}_{\mathrm{AF}} = m^{\alpha}_{\mathrm{AF}}/I^{\alpha}$, where $I^{\alpha} = \int_{-\infty}^{+\infty} \sum_{\sigma s} \rho^{\alpha}_{\sigma s}(\omega) d\omega/2$ is the total spectral weight of $\rho^{\alpha}_{\sigma s}(\omega)$. It allows one to investigate the contribution of the point-like spectrum of the Anderson localized states to the magnetization. This provides important information about the spectrum since with increasing disorder more and more one-particle states of the many-body system are transferred from the continuous to the point-like spectrum. For weak interactions ($U = 0.5$) the

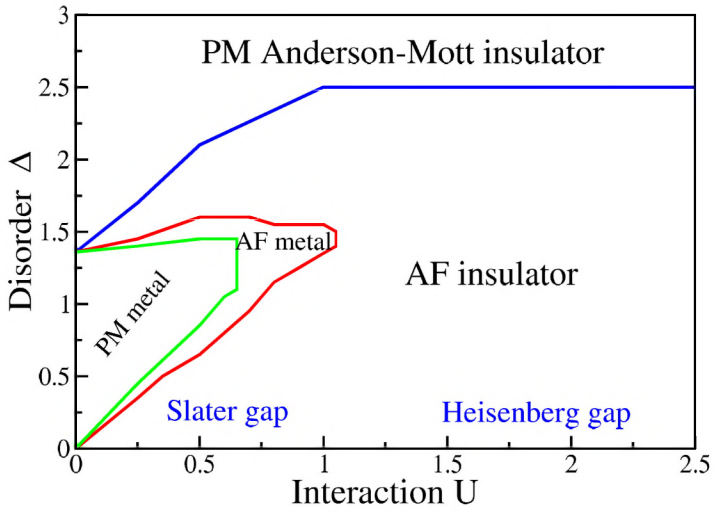

Fig. 1.4. Magnetic ground state phase diagram of the Anderson-Hubbard model at half-filling as calculated by DMFT with a spin resolved local DOS (see text); PM: paramagnetic, AF: antiferromagnetic; after Ref. 60.

decrease of the polarization with increasing disorder Δ obtained with geometric or arithmetic averaging is the same (see inset in Fig. 1.5). Since within arithmetic averaging all states are extended, the decrease of m^{α}_{AF} (which is also the same for the two averages in the limit of weak interactions, see lower panel of Fig. 1.5) must be attributed to disorder effects involving only the continuous spectrum. At larger U, the polarization is constant up to the transition from the AF insulator to the paramagnetic Anderson–Mott insulator. In the latter phase the polarization is undefined, because the continuous spectrum does not contribute to $I^{\mathrm{geom}}_{\mathrm{AF}}$.

In the absence of disorder the AF insulating phase has a small ("Slater") gap at $U/W < 1$ and a large ("Heisenberg") gap at $U/W > 1$. These limits can be described by perturbation expansions in U and $1/U$ around the symmetry broken state of the Hubbard and the corresponding Heisenberg model, respectively. In agreement with earlier studies[88] our results for m_{AF} (upper panel of Fig. 1.5) show that there is no sharp transition between these limits, even when disorder is present. This may be attributed to the fact that both limits are described by the same order parameter. However, the phase diagram (Fig. 1.4) shows that the two limits *can* be distinguished by their overall response to disorder. Namely, the reentrance of the AF

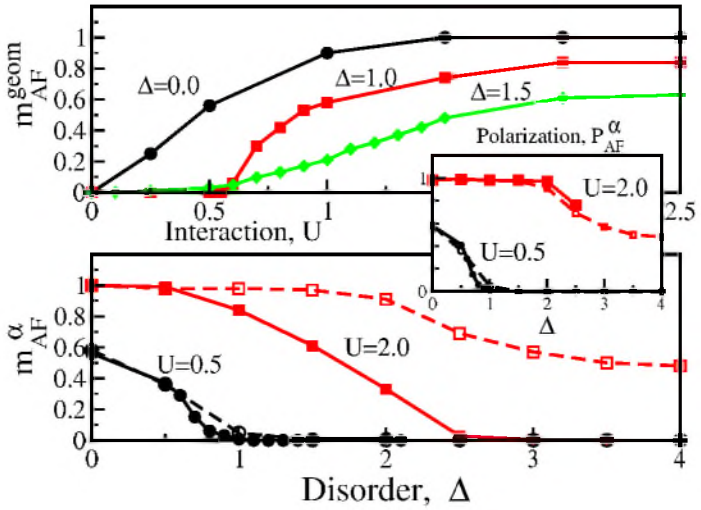

Fig. 1.5. Upper panel: Staggered magnetization $m^{\mathrm{geom}}_{\mathrm{AF}}$ as a function of interaction U. Lower panel: m^{α}_{AF}, α = geom/arith, as a function of disorder Δ (full lines: arithmetic average, dashed lines: geometric average). Inset: Polarization P^{α}_{AF} as a function of disorder.[60] Reprinted with permission from *Phys. Rev. Lett.* **102**, 146403 (2009). © American Physical Society.

metallic phase at $\Delta/W \gtrsim 1$ occurs only within the Slater AF insulating phase.

The magnetic structure of the Anderson–Mott insulator cannot be determined by the method used here since it describes only the continuous part of the spectra and not the point spectrum. However, only the paramagnetic solution should be expected to be stable because the kinetic exchange interaction responsible for the formation of the AF metal is suppressed by the disorder. This does not exclude the possibility of Griffiths phase-like AF domains.[89,90]

It is interesting to note that even the DMFT with an arithmetic average finds a disordered AF metal.[53,91] However, the arithmetically averaged local DOS incorrectly predicts both the paramagnetic metal and the AF metal to remain stable for arbitrarily strong disorder. Only a computational method which is sensitive to Anderson localization, such as the DMFT with geometrically averaged local DOS employed here, is able to detect the suppression of the metallic phase for $\Delta/W \gtrsim 1.5$ and the appearance of the paramagnetic Anderson–Mott insulator at large disorder Δ already on the one-particle level.

9. Summary

In this article we reviewed the properties of low-temperature quantum phases of strongly correlated, disordered lattice fermion systems with application to correlated electronic systems and ultracold fermions in optical lattices. We discussed the Anderson–Hubbard model and a comprehensive nonperturbative theoretical method for its solution, the DMFT combined with geometrical averaging over disorder. This approach provides a unified description of Anderson- and Mott-localization in terms of one-particle correlation functions.

We presented low-temperature quantum phase diagrams for the Anderson–Hubbard model at half filling, both in the paramagnetic and the antiferromagnetic phase. In the paramagnet, we observed re-entrant metal–insulator transitions induced by disorder and interaction, where the corresponding Anderson- and Mott-insulating phases are continuously connected. In the presence of antiferromagnetic order, a new antiferromagnetic metallic phase was found, which is stabilized by the interplay between interaction and disorder.

It is expected that these new quantum states will be observable by using ultracold fermions in optical lattices where disorder and interactions are easily tunable in a wide range. While current experimental temperatures are still above those required for observing quantum antiferromagnetism, the paramagnetic Mott–Anderson insulator should be easily accessible within current setups.

Even after several decades of research into the complex properties of disordered, interacting quantum many-body systems many fundamental problems are still unsolved. Future investigations of the existing open questions, and of the new questions which are bound to arise, are therefore expected to provide fascinating new insights.

Acknowledgments

We thank R. Bulla and S. Kehrein for useful discussions. Financial support by the SFB 484, TTR 80, and FOR 801 of the Deutsche Forschungsgemeinschaft is gratefully acknowledged.

References

1. P. W. Anderson, *Phys. Rev.* **109**, 1492 (1958).
2. E. Abrahams, P. W. Anderson, D. C. Licciardello and T. V. Ramakrishnan, *Phys. Rev. Lett.* **42**, 673 (1979).

3. L. P. Gor'kov, A. I. Larkin and D. E. Khmel'nitskii, *Zh. Eksp. Teor. Fiz. Pis'ma Red.* **30**, 248 (1979) [*JETP Lett.* **30**, 248 (1979)].
4. P. A. Lee and T. V. Ramakrishnan, *Rev. Mod. Phys.* **57**, 287 (1985).
5. D. Vollhardt and P. Wölfle, in *Electronic Phase Transitions*, eds. W. Hanke and Ya. V. Kopaev (North-Holland, Amsterdam, 1992), Chapter 1, p. 1.
6. A. Lagendijk, B. van Tiggelen and D. S. Wiersma, *Phys. Today* **62**, 24 (2009).
7. N. F. Mott, *Metal–Insulator Transitions*, 2nd edn. (Taylor and Francis, London 1990).
8. D. Belitz and T. R. Kirkpatrick, *Rev. Mod. Phys.* **66**, 261 (1994).
9. For a recent review of exact results on Anderson localization see: M. Disertori, W. Kirsch, A. Klein, F. Klopp and V. Rivasseau, *Panoramas et Synthèses* **25**, 1 (2008).
10. N. F. Mott, *Proc. Phys. Soc. A* **62**, 416 (1949).
11. H. V. Löhneysen, *Adv. Solid State Phys.* **40**, 143 (2000).
12. S. V. Kravchenko and M. P. Sarachik, *Rep. Prog. Phys.* **67**, 1 (2004).
13. A. M. Finkelshtein, *Sov. Phys. JEPT* **75**, 97 (1983).
14. C. Castellani, C. Di Castro, P. A. Lee and M. Ma, *Phys. Rev. B* **30**, 527 (1984).
15. M. A. Tusch and D. E. Logan, *Phys. Rev. B* **48**, 14843 (1993); *ibid.* **51**, 11940 (1995).
16. D. L. Shepelyansky, *Phys. Rev. Lett.* **73**, 2607 (1994).
17. P. J. H. Denteneer, R. T. Scalettar and N. Trivedi, *Phys. Rev. Lett.* **87**, 146401 (2001).
18. B. L. Altshuler and A. G. Aronov, in *Electron–Electron Interactions in Disordered Systems*, eds. M. Pollak and A. L. Efros (North-Holland, Amsterdam, 1985), p. 1.
19. E. Abrahams, S. V. Kravchenko and M. P. Sarachik, *Rev. Mod. Phys.* **73**, 251 (2001).
20. M. Lewenstein, A. Sanpera, V. Ahufinger, B. Damski, A. Sen De and U. Sen, *Adv. Phys.* **56**, 243 (2007).
21. I. Bloch, J. Dalibard and W. Zwerger, *Rev. Mod. Phys.* **80**, 885 (2008).
22. L. Fallani, J. E. Lye, V. Guarrera, C. Fort and M. Inguscio, *Phys. Rev. Lett.* **98**, 130404 (2007).
23. A. Aspect and M. Inguscio, *Phys. Today* **62**, 30 (2009).
24. L. Sanchez-Palencia and M. Lewenstein, *Nature Phys.* **6**, 87 (2010).
25. J. Billy, V. Josse, Z. Zuo, A. Bernard, B. Hambrecht, P. Lugan, D. Clément, L. Sanchez-Palencia, P. Bouyer and A. Aspect, *Nature* **453**, 891 (2008).
26. G. Roati, C. D'Errico, L. Fallani, M. Fattori, C. Fort, M. Zaccanti, G. Modugno, M. Modugno and M. Inguscio, *Nature* **453**, 895 (2008).
27. M. White, M. Pasienski, D. McKay, S. Q. Zhou, D. Ceperley and B. DeMarco, *Phys. Rev. Lett.* **102**, 055301 (2009).
28. D. Jaksch, C. Bruder, J. I. Cirac, C. W. Gardiner and P. Zoller, *Phys. Rev. Lett.* **81**, 3108 (1998).
29. M. Greiner, O. Mandel, T. Esslinger, T. W. Hänsch and I. Bloch, *Nature* **415**, 39 (2002).
30. W. Hofstetter, J. I. Cirac, P. Zoller, E. Demler and M. D. Lukin, *Phys. Rev. Lett.* **89**, 220407 (2002).

31. M. Köhl, H. Moritz, T. Stöferle, K. Günter and T. Esslinger, *Phys. Rev. Lett.* **94**, 080403 (2005).
32. S. Ospelkaus, C. Ospelkaus, O. Wille, M. Succo, P. Ernst, K. Sengstock and K. Bongs, *Phys. Rev. Lett.* **96**, 180403 (2006); K. Günter, T. Stöferle, H. Moritz, M. Köhl and T. Esslinger, *Phys. Rev. Lett.* **96**, 180402 (2006).
33. R. Jördens, N. Strohmaier, K. Günter, H. Moritz and T. Esslinger, *Nature* **455**, 204 (2008); U. Schneider, L. Hackermüller, S. Will, T. Best, I. Bloch, T. A. Costi, R. W. Helmes, D. Rasch and A. Rosch, *Science* **322**, 1520 (2008).
34. The most probable value of a random quantity is defined as that value for which its PDF becomes maximal.
35. E. Limpert, W. A. Stahel and M. Abbt, *BioScience* **51**, 341 (2001).
36. E. L. Crow and K. Shimizu (eds.), *Log-Normal Distribution-Theory and Applications* (Marcel Dekker, Inc., New York, 1988).
37. A. D. Mirlin and Y. V. Fyodorov, *Phys. Rev. Lett.* **72**, 526 (1994); *J. Phys. I France* **4**, 655 (1994).
38. M. Janssen, *Phys. Rep.* **295**, 1 (1998).
39. G. Schubert, A. Weiße and H. Fehske in *High Performance Computing in Science and Engineering Garching 2004*, eds. A. Bode, F. Durst (Springer Verlag, 2005), pp. 237–250.
40. F. Evers and A. D. Mirlin, *Rev. Mod. Phys.* **80**, 1355 (2008).
41. A. Richardella, P. Roushan, S. Mack, B. Zhou, D. A. Huse, D. D. Awschalom and A. Yazdani, *Science* **327**, 665 (2010).
42. G. Schubert, J. Schleede, K. Byczuk, H. Fehske and D. Vollhardt, *Phys. Rev. B* **81**, 155106 (2010).
43. D. Lloyd, *J. Phys. C: Solid State Phys.* **2**, 1717 (1969).
44. D. Thouless, *Phys. Rep.* **13**, 93 (1974).
45. F. Wegner, *Z. Phys. B* **44**, 9 (1981).
46. E. W. Montroll and M. F. Schlesinger, *J. Stat. Phys.* **32**, 209 (1983).
47. M. Romeo, V. Da Costa and F. Bardou, *Eur. Phys. J. B* **32**, 513 (2003).
48. V. Dobrosavljević and G. Kotliar, *Phys. Rev. Lett.* **78**, 3943 (1997); *Philos. Trans. R. Soc. London, Ser. A* **356**, 57 (1998).
49. V. Dobrosavljević, A. A. Pastor and B. K. Nikolić, *Europhys. Lett.* **62**, 76 (2003).
50. W. Metzner and D. Vollhardt, *Phys. Rev. Lett.* **62**, 324 (1989).
51. A. Georges, G. Kotliar, W. Krauth and M. J. Rozenberg, *Rev. Mod. Phys.* **68**, 13 (1996).
52. G. Kotliar and D. Vollhardt, *Phys. Today* **57**, 53 (2004).
53. M. Ulmke, V. Janiš and D. Vollhardt, *Phys. Rev. B* **51**, 10411 (1995).
54. R. Vlaming and D. Vollhardt, *Phys. Rev. B* **45**, 4637 (1992).
55. Y. Song, R. Wortis and W. A. Atkinson, *Phys. Rev. B* **77**, 054202 (2008).
56. F. X. Bronold, A. Alvermann and H. Fehske, *Philos. Mag.* **84**, 637 (2004).
57. M.-T. Tran, *Phys. Rev. B* **76**, 245122 (2007).
58. K. Byczuk, W. Hofstetter and D. Vollhardt, *Phys. Rev. Lett.* **94**, 056404 (2005).
59. K. Byczuk, *Phys. Rev. B* **71**, 205105 (2005).
60. K. Byczuk, W. Hofstetter and D. Vollhardt, *Phys. Rev. Lett.* **102**, 146403 (2009).

61. M. C. O. Aguiar, V. Dobrosavljević, E. Abrahams and G. Kotliar, *Phys. Rev. Lett.* **102**, 156402 (2009).
62. G. Roux, T. Barthel, I. P. McCulloch, C. Kollath, U. Schollwöck and T. Giamarchi, *Phys. Rev. A* **78**, 023628 (2008).
63. U. Bissbort and W. Hofstetter, *Europhys. Lett.* **86**, 50007 (2009).
64. U. Bissbort, R. Thomale and W. Hofstetter, preprint arXiv:0911.0923.
65. L. Pollet, N. V. Prokof'ev, B. V. Svistunov and M. Troyer, *Phys. Rev. Lett.* **103**, 140402 (2009).
66. D. Semmler, K. Byczuk and W. Hofstetter, *Phys. Rev. B* **81**, 115111 (2010).
67. J. T. Stewart, J. P. Gaebler and D. S. Jin, *Nature* **454**, 744 (2008).
68. T.-L. Dao, A. Georges, J. Dalibard, C. Salomon and I. Carusotto, *Phys. Rev. Lett.* **98**, 240402 (2007).
69. P. T. Ernst, S. Götze, J. S. Krauser, K. Pyka, D.-S. Lühmann, D. Pfannkuche and K. Sengstock, preprint arXiv:0908.4242.
70. N. Fabbri, D. Clément, L. Fallani, C. Fort, M. Modugno, K. M. R. van der Stam and M. Inguscio, *Phys. Rev. A* **79**, 043623 (2009).
71. R. Abou-Chacra, D. J. Thouless and P. W. Anderson, *J. Phys. C: Solid State Phys.* **6**, 1734 (1973).
72. K. Efetov, *Supersymmetry in Disorder and Chaos* (Cambridge University Press, Cambridge, 1997).
73. E. Müller–Hartmann, *Z. Phys. B* **74**, 507 (1989).
74. J. K. Freericks and V. Zlatić, *Rev. Mod. Phys.* **75**, 1333 (2003).
75. J. K. Freericks, *Transport in Multilayered Nanostructures — The Dynamical Mean-Field Approach* (Imperial College Press, London, 2006).
76. D. Heidarian and N. Trivedi, *Phys. Rev. Lett.* **93**, 126401 (2004).
77. H. Shinaoka and M. Imada, *Phys. Rev. Lett.* **102**, 016404 (2009).
78. A. Alvermann and H. Fehske, *Eur. Phys. J. B* **48**, 295 (2005).
79. B. Bulka, B. Kramer and A. MacKinnon, *Z. Phys. B* **60**, 13 (1985); B. Bulka, M. Schreiber and B. Kramer, *Z. Phys. B* **66**, 21 (1987).
80. E. Z. Kuchinskii, I. A. Nekrasov and M. V. Sadovskii, *JETP* **106**, 581, (2008); E. Z. Kuchinskii, N. A. Kuleeva, I. A. Nekrasov and M. V. Sadovskii, *J. Exp. and Theor. Phys.* **110**, 325 (2010).
81. P. Henseler, J. Kroha and B. Shapiro, *Phys. Rev. B* **77**, 075101 (2008); *Phys. Rev. B* **78**, 235116 (2008).
82. V. Janiš and D. Vollhardt, *Phys. Rev. B* **63**, 125112 (2001).
83. V. Janiš and J. Kolorenč, *Phys. Rev. B* **71**, 033103 (2005); *Phys. Rev. B* **71**, 245106 (2005).
84. The order parameter $m_{\mathrm{AF}}^{\mathrm{geom}}$ is related to the *number* of states in the continuous part of the spectrum and thus accounts for the existence of itinerant quasiparticles which then order magnetically. A finite value of $m_{\mathrm{AF}}^{\mathrm{geom}}$ corresponds to a spin density wave, which should be observable in neutron scattering experiments.
85. K. G. Wilson, *Rev. Mod. Phys. A* **47**, 773 (1975); W. Hofstetter, *Phys. Rev. Lett. A* **85**, 1508 (2000); R. Bulla, T. Costi and T. Pruschke, *Rev. Mod. Phys. A* **80**, 395 (2008).
86. R. Bulla, T. A. Costi and D. Vollhardt, *Phys. Rev. B* **64**, 045103 (2001).

87. K. Byczuk, W. Hofstetter and D. Vollhardt, *Physica B* **359–361**, 651 (2005).
88. T. Pruschke, *Prog. Theo. Phys. Suppl.* **160**, 274 (2005).
89. R. B. Griffiths, *Phys. Rev. Lett.* **23**, 17 (1969).
90. V. Dobrosavljević and E. Miranda, *Phys. Rev. Lett.* **94**, 187203 (2005).
91. A. Singh, M. Ulmke and D. Vollhardt, *Phys. Rev. B* **58**, 8683 (1998).